

Random motility regulation drives the fragmentation of microbial ecosystems

Alberto Dinelli,^{1,2} Ada Altieri,^{2,*} and Julien Tailleur^{3,*}

¹*Department of Biochemistry, University of Geneva, 1211 Geneva, Switzerland*

²*Université Paris Cité, MSC, UMR 7057 CNRS, 75013 Paris, France*

³*Department of Physics, Massachusetts Institute of Technology, Cambridge, Massachusetts 02139, USA*

(Dated: March 18, 2025)

The self-organization of microbial ecosystems involves a large variety of mechanisms, ranging from biochemical signaling to population dynamics. Among these, the role of motility regulation has been little studied, despite the importance of active migration processes. Here we show how weak, random motility regulation generically induces the fragmentation of bacterial ecosystems comprising a large number of coexisting strains. To do so, we simulate microscopic models of run-and-tumble bacteria whose self-propulsion speeds are regulated by the local density of each strain. Our simulations reveal that, as the heterogeneity of the interaction network increases, the ecosystem undergoes a phase transition leading to the emergence of distinct communities. To account for these results and assess their robustness, we use random-matrix theory to analyze the hydrodynamic description of the bacterial ecosystem, obtaining a quantitative agreement with our microscopic simulations. Our results are shown to hold for a variety of motility-regulation mechanisms and should be relevant to the study of community formation by motile organisms.

How ecosystems self-organize into diverse coexisting communities is an open problem in ecology that involves a variety of mechanisms as diverse as speciation [1, 2], migration [3–5], interaction with the environment [6–10], or competition for resources [11–14]. In this context, microbial ecosystems have received a lot of attention, both because of their abundance in nature and because they offer a controlled setting to study community formation [13, 15–19].

A lot of progress has been made using low-dimensional ecosystems, in which a small number of strains coexist [20–23]. Much focus has been brought on how genetic drift, by which the random extinction of bacterial strains impacts the local composition of the colony, induces genetic sectoring and community formation [24, 25]. In addition, competition for resources or mutualistic interactions that impact growth rates have also been extensively studied since the work of Lotka and Volterra [26, 27].

Recently, progress has been made in the study of more realistic, high-dimensional ecosystems, that comprise a large number of coexisting species. This is an important challenge since it is unclear when lessons from the low-dimensional limit generalize to complex ecosystems [28, 29]. For instance, studies have shown that high-dimensional generalizations of the Lotka-Volterra and Resource-Consumer models display complex attractors that cannot be extrapolated from low-dimensional systems [30–37], suggesting that, in ecology also, “more is different” [38].

While there are many established results on how population dynamics lead to community formation, far less is known about the role of motility. This is somewhat surprising since motility regulation, in the form of chemotactic [39] or quorum-sensing [40, 41] interactions,

has been established as a powerful pattern-formation pathway. In low-dimensional ecosystems, it has for instance been shown that a sufficiently strong reciprocal motility inhibition or enhancement between coexisting strains respectively leads to their colocalization or demixing [42]. In high-dimensional ecosystems, however, the role played by motility remains uncharted territory. There, in addition to specific quorum-sensing signaling pathways, motility regulation also emerges as a byproduct of metabolic interactions, whereby bacteria exchange metabolites such as vitamins, amino acids, nucleotides, growth factors [43, 44]. The energetic cost associated with producing and processing these metabolites is expected to have a mild, random impact on all other cell functions, including motility [45].

In this article, we show theoretically and numerically that such a weak and random motility regulation between strains suffices to drive the fragmentation of high-dimensional ecosystems, leading to a diverse set of coexisting communities. Remarkably, this happens even in the presence of pre-existing attractive interactions between strains: a gregarious community—where all strains coexist—is also fragmented upon adding weak random motility regulation. To demonstrate our results, we first introduce below a model to account for random motility regulation between N strains of run-and-tumble bacteria [46], which we study numerically in two spatial dimensions. Namely, the self-propulsion speed of strain μ is chosen to depend on the local density of all strains, $v_\mu[\{\rho_\nu\}]$ (Fig. 1a-b). Our key result is that, when $\{\partial_{\rho_\nu} v_\mu\}$ forms a set of random numbers of variance $\sim \sigma^2/N$, the system undergoes a fragmentation transition as σ^2 increases (Fig. 1c). To account for this transition, we coarse-grain our microscopic model and employ random-matrix theory to characterize the phase behavior predicted by the resulting hydrodynamic theory, in the spirit of [47–50]. We then validate our results using extensive numerical simulations in one space dimension.

* Corresponding authors. Email: ada.altieri@u-paris.fr and jgt@mit.edu

Finally, we show the robustness of our results by considering different mechanisms leading to motility regulation, including both reciprocal and non-reciprocal interactions, as well as different topologies of the interaction network.

I. RANDOM-MOTILITY-REGULATION MODEL

We consider $N \gg 1$ strains of bacteria, whose motions alternate between runs and tumbles. During a run phase, bacteria i of strain μ self-propels with fixed orientation $\mathbf{u}_{i,\mu}$ so that its position evolves as $\dot{\mathbf{r}}_{i,\mu} = v_{i,\mu} \mathbf{u}_{i,\mu}$. Tumble events correspond to full randomizations of the bacteria's orientations, and occur with a constant rate τ^{-1} . As shown in Fig. 1a, motility regulation is modeled by making the self-propulsion speed $v_{i,\mu}$ depend on the local density $\{\rho_\nu\}$ of all strains: $v_{i,\mu} \equiv v_\mu(\mathbf{r}_{i,\mu}, [\{\rho_\nu\}])$. Specifically, we choose:

$$v_\mu(\mathbf{r}_{i,\mu}, [\{\rho_\nu\}]) = v_0 \mathcal{S} \left(\sum_{\nu=1}^N \kappa_{\mu\nu} \frac{\tilde{\rho}_\nu(\mathbf{r}_i) - \bar{\rho}}{\varphi} \right), \quad (1)$$

where \mathcal{S} is a sigmoidal function and the density is measured locally as $\tilde{\rho}_\nu \equiv K * \rho_\nu$, with K a convolution kernel representing the transport of signaling molecules or metabolites (See Methods for details). We set the unit of length such that the range of K is $\ell_{\text{int}} = 1$. The density $\bar{\rho}$ represents the typical density around which motility regulation impacts the self-propulsion speed while φ controls the density range over which bacteria are sensitive to motility regulation. Finally, the matrix $\kappa_{\mu\nu}$ determines the specific interaction between strains μ and ν , i.e. how strain ν enhances ($\kappa_{\mu\nu} > 0$) or inhibits ($\kappa_{\mu\nu} < 0$) the self-propulsion speed of strain μ . This is depicted schematically in Fig. 1b. We note that our results are robust to the precise choice for the functional form Eq. (1), as discussed in Section IV.

In most of this article, we model the random motility-regulation using independent Gaussian distributed $\kappa_{\mu\nu}$. This allows for analytical progress, but, as often with random-matrix theory, we expect that our results extend to distributions with finite means and variances [32]. The distribution of $\kappa_{\mu\nu}$ is then entirely determined by its first two moments, which we define as:

$$\langle \kappa_{\mu\nu} \rangle = \frac{m}{N}, \quad \text{Var}[\kappa_{\mu\nu}] = \frac{\sigma^2}{N}. \quad (2)$$

We first note that the scaling of the average simply ensures that the sum in Eq. (1) remains finite in the large N limit. The scaling of the variance will prove to be such that the fragmentation transition occurs for $\sigma^2 \sim \mathcal{O}(1)$: *weak* random motility regulation thus suffices to drive community formation. Different scalings can then be extrapolated by sending σ^2 to 0 or ∞ , as has been done for the generalized Lotka-Volterra (GLV) model [51]. For generality, we allow $m \neq 0$ to model a possible average

inhibition ($m < 0$) or enhancement ($m > 0$) of the self-propulsion speed that could result from the systematic effect of metabolic or quorum-sensing interactions.

II. NUMERICAL SIMULATIONS IN 2D

To understand how random motility regulation impacts the large-scale behavior of the system, we start by performing $2d$ simulations of the bacterial dynamics described above (see Methods for details). In simulations, we vary the average inter-strain motility inhibition m and the interaction heterogeneity σ^2 . As we show in Fig. 1c, a rich variety of phases emerge from random motility regulation.

We first show results for an ecosystem without systematic regulation ($m = 0$) in the top panels of Fig. 1c. In the monodisperse case ($\sigma^2 = 0$) the homogeneous phase is stable. Upon increasing σ^2 , we observe a transition into a fragmented ecosystem: the steady state is phase separated and comprises coexisting communities that differ in strain composition.

To test whether random motility regulation can compete with a pre-existing self-organization of the colony, we consider the case of systematic motility inhibition ($m < 0$) in the bottom panels of Fig. 1c. In the monodisperse case, a gregarious phase is observed when m is sufficiently negative: There, all species equally participate to a motility-induced phase separation [42, 52]. Upon increasing σ^2 , the colony transitions again into a fragmented ecosystem, hence overcoming the aggregation induced by $m < 0$. A weak, random motility regulation is thus sufficient to drive community formation in microbial ecosystems, both in the absence and in the presence of a pre-existing self-organization. Note that, for a given choice of (m, σ^2) , the emergent behavior described above is robustly observed across simulations with different realization of the random coefficients $\{\kappa_{\mu\nu}\}$.

To characterize the transition to fragmented ecosystems, we first measure the histograms of the local density fields $\rho_\mu(\mathbf{r})$, as well as that of the total density $\rho_t \equiv N^{-1} \sum_\nu \rho_\nu$. The corresponding measurements are shown in Figs. 1d-f. When random motility regulation is introduced in a non-interacting system, Fig. 1d, the emergence of the fragmented phase is reflected in the bimodal nature of the single-strain distributions $p(\rho_\nu)$. The total density, however, remains essentially homogeneous and $p(\rho_t)$ is barely altered. The fragmentation transition then resembles a demixing transition. On the contrary, the gregarious phase observed in a monodisperse system, Fig. 1e, leads to two peaks in the histogram $p(\rho_t)$, identical to those observed at the single-species level. Finally, when heterogeneity is introduced in a gregarious system, Fig. 1f, one both observes a reminiscence of the global phase separation in $p(\rho_t)$ and a rich variety of distributions at the single-strain level $p(\rho_\nu)$: the system experiences a combination of demixing and phase separation.

To better characterize the difference between the gre-

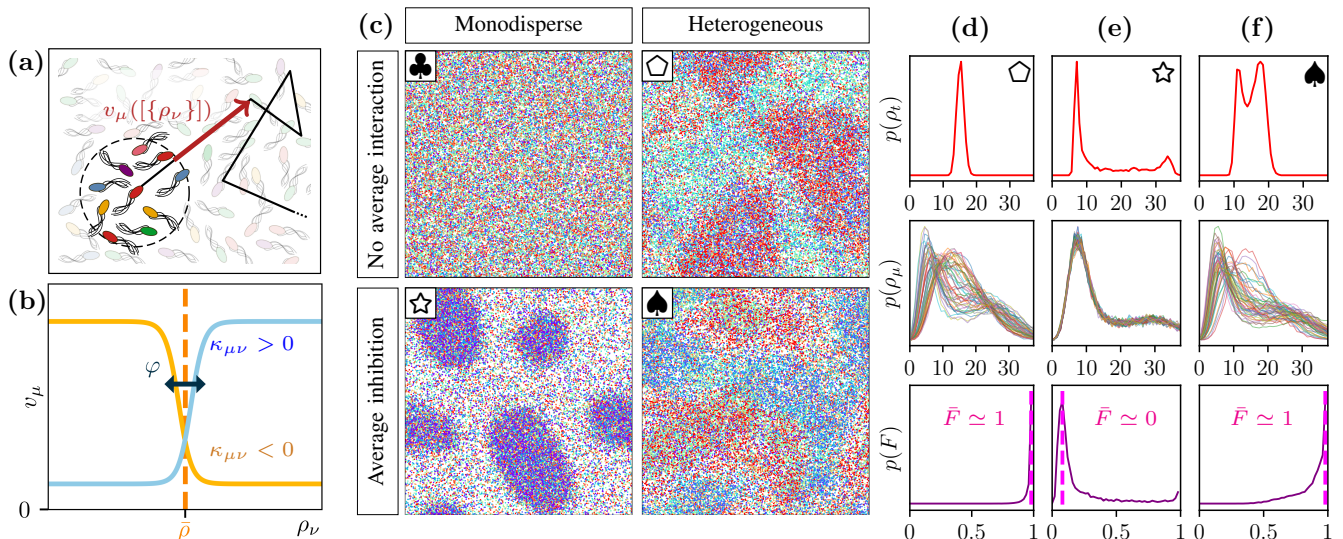


FIG. 1. **From random motility regulation to community formation.** (a) Sketch of the run-and-tumble dynamics and of the motility regulation mechanism. The different colors correspond to the N different strains and the speed v_μ of strain μ depends on the local density of bacteria in each strain. (b) Motility regulation of strain μ by strain ν through Eq. (1), when all strains but ν have density $\bar{\rho}$. (c) Snapshots from 2d microscopic simulations with $N = 50$ strains for a random realization of $\{\kappa_{\mu\nu}\}$. Particles of the same strain have the same color. For clarity, we show 10 strains out of 50. Top panels (\clubsuit , \diamond): Phase behavior in the absence of average motility regulation, $m = 0$. (\clubsuit): In the noninteracting limit $\sigma^2 = 0$, the system is homogeneous. (\diamond): A fragmented ecosystem emerges upon increasing the heterogeneity ($\sigma^2 = 2$). Bottom panels (\star , \spadesuit): Simulations with average motility inhibition $m = -1$. (\star): We observe gregarious phase separation in the monodisperse limit ($\sigma^2 = 0$). (\spadesuit): Increasing heterogeneity again leads to fragmentation and community formation ($\sigma^2 = 2$). Parameters common to all panels: $L_x = L_y = 16$, $\rho_0 = 15$, $\bar{\rho} = 15$, $\varphi = 10$, $v_0 = 1$, $\tau_0 = 1$. (d-f) Statistical analysis performed on simulations from panel (c). Top row: Histograms of the total density ρ_t . The overall modulation of the ecosystem density stems only from the average motility inhibition (e) and recedes upon increasing heterogeneity (f). Central row: Each single-strain density histogram is shown using a different color; Heterogeneity suffices to induce single-strain phase separation (d). Bottom row: Histograms of the fragmentation parameter F and most probable value \bar{F} , which show the transition to fragmentation as heterogeneity increases.

gregarious and fragmented ecosystems, we then introduce a fragmentation order parameter. To do so, we first consider local density fluctuations $\delta\rho(\mathbf{r}) = (\delta\rho_1, \dots, \delta\rho_N)$, where $\delta\rho_\mu(\mathbf{r}) \equiv \rho_\mu(\mathbf{r}) - \rho_0$. In the perfectly gregarious case at $\sigma^2 = 0$, all fluctuations $\delta\rho_\mu(\mathbf{r})$ occur synchronously in space, so that $\delta\rho(\mathbf{r})$ is parallel to $\hat{\mathbf{1}} = (1, \dots, 1)/\sqrt{N}$. On the contrary, in the fragmented case, density fluctuations of non-coexisting strains have opposite signs.

To distinguish these two scenarios, we thus use the relative angle between $\delta\rho(\mathbf{r})$ and $\hat{\mathbf{1}}$, as was done to characterize equilibrium phase-separation in multi-component systems [47, 48]. This leads us to define a fragmentation order-parameter field as:

$$F[\mathbf{r}] \equiv 1 - \cos^2 \theta(\mathbf{r}), \quad \cos^2 \theta(\mathbf{r}) = \frac{|\delta\rho(\mathbf{r}) \cdot \hat{\mathbf{1}}|^2}{|\delta\rho(\mathbf{r})|^2}. \quad (3)$$

When $F(\mathbf{r}) \approx 1$, the system is thus locally fragmented, while $F(\mathbf{r}) \approx 0$ corresponds to a locally gregarious behavior. We report the histogram of $F(\mathbf{r})$ in the bottom panels of Fig. 1d-e. As expected, $p(F)$ is peaked close to

0 in the gregarious phase (d) whereas it is peaked close to 1 in the fragmented case (e). The fragmentation parameter F is thus a relevant order parameter to distinguish gregarious and fragmented communities.

Our simulations thus demonstrate the existence of a phase transition towards a fragmented ecosystem upon increasing the heterogeneity of random motility-regulation interactions. We now develop a theoretical framework to elucidate the physical origin of this transition, starting from the bacteria microscopic dynamics.

III. THEORY

Standard methods [53] show that, at the macroscopic scale, the run-and-tumble dynamics lead to a diffusive behavior and the evolution of the density field of strain μ reads

$$\partial_t \rho_\mu = \nabla_{\mathbf{r}} \cdot [M_\mu \nabla_{\mathbf{r}} \mathbf{u}_\mu], \quad (4)$$

where $M_\mu = \rho_\mu v_\mu^2 \tau / d$ is the collective mobility of strain μ , d the number of space dimensions, and $\mathbf{u}_\mu =$

$\log v_\mu(\{\rho_\nu(\mathbf{r})\}) + \log \rho_\mu(\mathbf{r})$ plays the role of an effective chemical potential. The entropic contribution $\log \rho_\mu$ accounts for the random-walk nature of run-and-tumble dynamics that favors homogeneous steady states. On the contrary, the excess chemical potential $\log v_\mu(\mathbf{r}, \{\rho_\nu\})$ stems from the motility regulation and reflects the tendency of bacteria to accumulate where they move slower.

To predict the instability of homogeneous states, we first note that, when the variations of the density field occurs on scales much larger than the interaction length, we can use a local approximation to the self-propulsion speed: $v_\mu(\mathbf{r}) = v_\mu(\{\rho_\nu(\mathbf{r})\})$. We then perform a linear-stability analysis of the corresponding ‘local’ field theory around a well-mixed homogeneous state: $\boldsymbol{\rho}_0 \equiv \rho_0(1, \dots, 1)$. In Fourier space, the linearized dynamics of a density fluctuation reads: $\partial_t \delta \hat{\rho}_\mu(\mathbf{q}) = -q^2 \mathcal{D}_{\mu\nu} \delta \hat{\rho}_\nu(\mathbf{q})$, where \mathbf{q} denotes the Fourier mode and $\mathcal{D}_{\mu\nu}$ is a diffusivity matrix given by:

$$\mathcal{D}_{\mu\nu} = \mathcal{D}_\mu^0 \left[\delta_{\mu\nu} + \rho_0 \frac{\partial \log v_\mu}{\partial \rho_\nu} \right], \quad \mathcal{D}_\mu^0 = \frac{v_\mu(\boldsymbol{\rho}_0)^2 \tau}{d}. \quad (5)$$

In the absence of motility-regulation, Eq. (5) amounts to N independent diffusion equations with diffusivity \mathcal{D}_μ^0 . Motility regulation couples the dynamics of all strains through the terms $\partial_{\rho_\nu} \log v_\mu$. A homogeneous well-mixed state becomes unstable when the eigenvalue of $\mathcal{D}_{\mu\nu}$ with the smallest real part, denoted by λ_0 , satisfies $\text{Re}(\lambda_0) < 0$. The corresponding normalized eigenvector $\hat{\mathbf{e}}_0$ can then be used to estimate the fragmentation parameter as

$$F[\hat{\mathbf{e}}_0] = 1 - |\hat{\mathbf{e}}_0 \cdot \hat{\mathbf{1}}|^2. \quad (6)$$

To make progress analytically, we consider the case $\rho_0 = \bar{\rho}$, which leads to a diffusivity matrix $\mathcal{D}_{\mu\nu}$ given by:

$$\mathcal{D}_{\mu\nu} = \mathcal{D}_0 \left(\delta_{\mu\nu} + \frac{\bar{\rho}}{\varphi} \kappa_{\mu\nu} \right), \quad (7)$$

where $\mathcal{D}_0 = v_0^2 \tau / d$. Equation (7) then allows us to characterize analytically the spectrum of $\mathcal{D}_{\mu\nu}$ using results from random-matrix theory [54–57]. Furthermore, we first focus on the case of symmetric interactions $\kappa_{\mu\nu} = \kappa_{\nu\mu}$, which make the eigenvalues λ_i of \mathcal{D} real. We note that these specific choices do not restrict the scope of our results: in the Supplementary Material we extend our analysis to $\rho_0 \neq \bar{\rho}$ and discuss the spectral properties of $\mathcal{D}_{\mu\nu}$ in the presence of asymmetric interactions. Let us now show how, starting from Eq. (7), we can predict the phase diagrams presented in Fig. 2.

A. The fragmentation transition

To study the onset of the fragmentation transition, we consider the spectral density of eigenvalues $\mu(\lambda) \equiv \lim_{N \rightarrow \infty} \frac{1}{N} \sum_{i=1}^N \langle \delta(\lambda - \lambda_i) \rangle$, where $\langle \cdot \rangle$ denotes the average

over the realizations of $\kappa_{\mu\nu}$. We can use Eq. (7) to infer the spectral density of the diffusivity matrix from that of the GOE matrix $\kappa_{\mu\nu}$ [58].

In the absence of pre-existing self-organization ($m = 0$), the result is a shifted Wigner semicircle [59], centered at $\lambda = \mathcal{D}_0$, and of radius $2\mathcal{D}_0 \bar{\rho} \sigma / \varphi$. The homogeneous phase is then predicted to be linearly unstable whenever the heterogeneity σ^2 is large enough:

$$\sigma^2 > \frac{\varphi^2}{2\bar{\rho}^2}. \quad (8)$$

Furthermore, random-matrix theory tells us that the eigenvectors of \mathcal{D} are uniformly distributed on the unit sphere. They are thus generically orthogonal to $\hat{\mathbf{1}}$ and the perturbations $\{\delta \rho_\mu\}$ are such that $\sum_\mu \delta \rho_\mu = 0$: the system undergoes demixing between communities with different strain compositions and the fragmentation parameter is $F = 1$. We report in Fig. 2(a) the phase diagram predicted by the transition line Eq. (8), together with illustrative plots for the spectral density and the eigenvector components.

When an average self-inhibition is present ($m < 0$), the spectrum of $\mathcal{D}_{\mu\nu}$ comprises both the shifted Wigner semicircle and a Gaussian-distributed outlier centered at $\lambda_0 = \mathcal{D}_0 [1 + (m + \sigma^2/m)\bar{\rho}/\varphi]$, as shown in the left inset of Fig. 2b. As $N \rightarrow \infty$, the outlier becomes delta-distributed. There are then two different scenarios. For small heterogeneity, $\sigma^2 < m^2$, the outlier is outside of the Wigner semi-circle, and is the smallest eigenvalue. The homogeneous phase is then unstable whenever:

$$\bar{\rho} \sigma^2 > -m\varphi - m^2 \bar{\rho}. \quad (9)$$

The eigenvector associated to the outlier has been characterized [57] and satisfies $\hat{\mathbf{e}}_0 \cdot \hat{\mathbf{1}} = \sigma/|m|$ so that $F = \sigma^2/m^2$. For $\sigma = 0$, we recover a gregarious phase with $F = 0$ while the ecosystem becomes increasingly fragmented as σ^2 increases. At $\sigma^2 = m^2$, the BBP transition occurs [54, 55] and the Wigner semicircle swallows the outlier. The physics of the system is then entirely determined by the weak random-motility regulation. The transition occurs again when Eq. (8) is satisfied and $F = 1$. The transition lines corresponding to these two scenarios, together with illustrative spectral densities and eigenvectors, are shown in Fig. 2(b). The colormap for the fragmentation parameter F highlights how, upon increasing the heterogeneity σ^2 , fragmentation overrules any pre-existing form of organization.

Random-matrix theory thus predicts how weak random motility regulation generically leads to the formation of fragmented ecosystem both in the presence and in the absence of pre-existing self-organization. These results are in qualitative agreement with the 2d numerical results shown in Fig. 1 and 2. We note that these predictions hold in the $N \rightarrow \infty$ limit, which is hard to statistically characterize in 2d. We thus now present results of extensive numerical simulations in 1d that allow

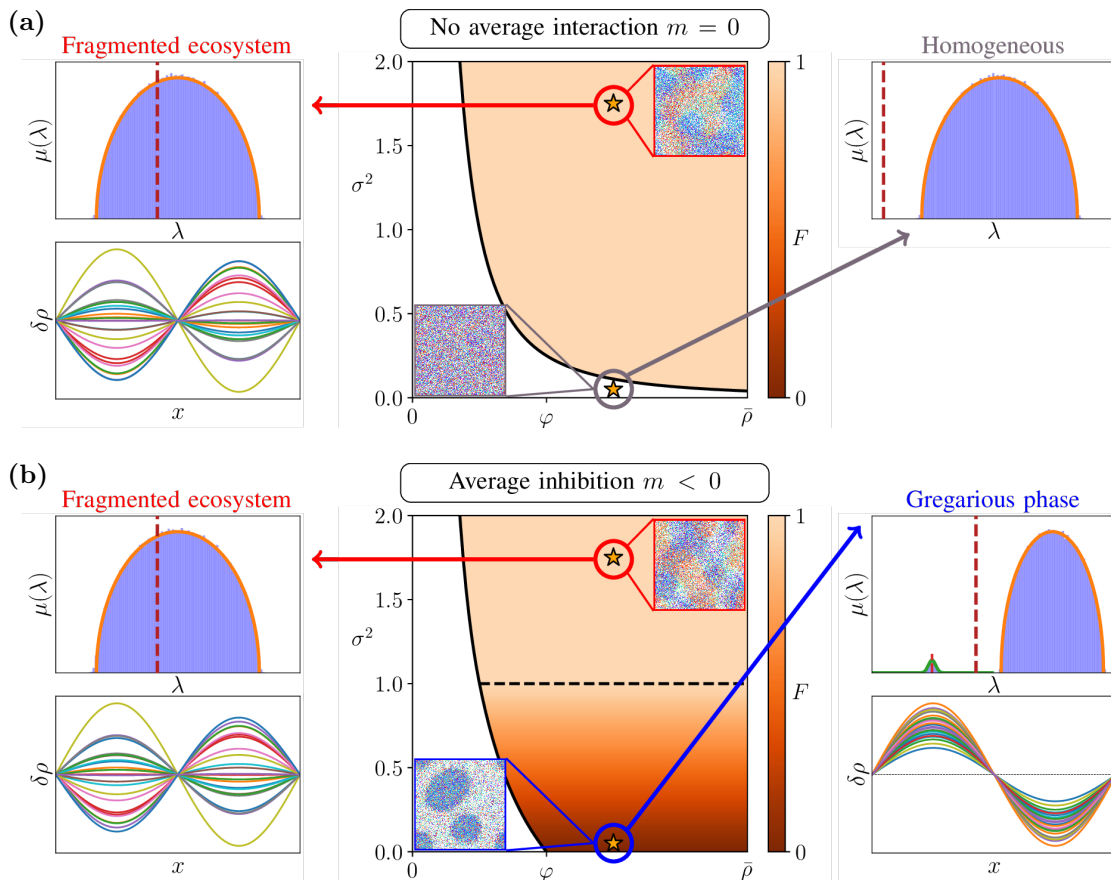


FIG. 2. **Phase diagrams of the fragmentation transition in the $(\bar{\rho}, \sigma^2)$ space for symmetric interactions $\kappa_{\mu\nu} = \kappa_{\nu\mu}$.** Panels (a) and (b) correspond to the presence and the absence of average motility inhibition, respectively. White regions represent stable homogeneous phases, while shaded regions correspond to phase-separated states. The color encodes the value of the fragmentation order parameter F predicted by Eq. (6), which ranges from 0 in gregarious ecosystems to 1 in fragmented ones. For each phase diagram, we consider two illustrative points (Stars). For each, we first show in inset a steady-state snapshot of the system. For clarity, we show 25 out of $N = 100$ strains in each snapshot. We then also plot the spectral densities $\mu(\lambda)$ predicted theoretically (orange and green lines) and computed numerically (lilac histogram). The dashed red line indicates the instability threshold $\lambda = 0$. When the system is predicted to be unstable, we plot the density modulation corresponding to the most unstable eigenvector $\hat{\mathbf{e}}_0$. (a) For $m = 0$, Eq. (8) (black line) predicts a transition from homogeneous to fragmented ecosystems for large enough σ^2 . The system enters the fragmented phase when the left edge of the Wigner semicircle $\mu(\lambda)$ falls below 0. The associated eigenvector $\hat{\mathbf{e}}_0$ is orthogonal to $(1, \dots, 1)$, corresponding to a spatial demixing of the strains. (b) For $m < 0$, the system is first gregarious at small σ^2 and becomes increasingly fragmented as the heterogeneity increases towards the BBP transition line at $\sigma^2 = m^2$ where $F = 1$ (dashed line). The boundaries of the homogeneous phase (solid lines) are predicted by Eq. (8) and Eq. (9) for $\sigma^2 > m^2$ and $\sigma^2 < m^2$, respectively. For $\sigma^2 < m^2$, the spectral density includes an outlier located to the left of the Wigner semicircle (top right inset), which first becomes unstable. At $\sigma^2 = 0$, the associated eigenvector is $\hat{\mathbf{e}}_0 \propto (1, \dots, 1)$, leading to a gregarious dynamics. For $\sigma^2 > m^2$, the Wigner semicircle has swallowed the outlier and $\hat{\mathbf{e}}_0 \cdot \hat{\mathbf{1}} = 0$.

testing more precisely the transition lines.

B. Quantitative test using 1d numerical simulation

To characterize the transition to community formation, we simulate $N = 100$ species on a domain of length $L_x = 30$, fixing the density per species at $\rho_0 = \bar{\rho}$. We explore the phase diagrams of Fig. 2 by varying the values of (m, σ^2) . For each point in the phase diagram, we

perform $K = 15$ simulations and build the single-strain density distribution $p(\rho_\mu)$ and the total-density distribution $p(\rho_t)$. As in Sec. II, the presence of multiple peaks in $p(\rho_t)$ and $p(\rho_\mu)$ corresponds to phase separation for the total density and for individual strains, respectively. We thus use the standard deviation of these distributions as an indicator for phase separation. We normalize the standard deviations of the total and single-strain densities such that $\Delta\rho_t = 1$ and $\langle \Delta\rho_\mu \rangle = 1$ correspond to the Poissonian fluctuations of a homogeneous system.

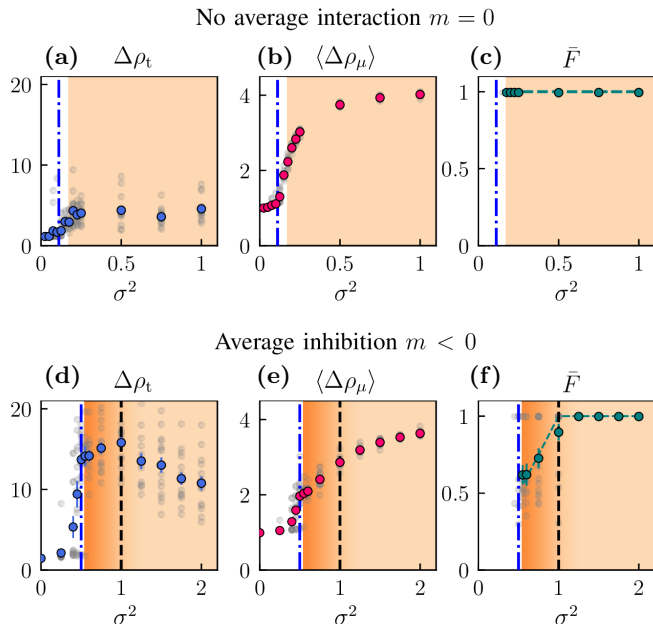


FIG. 3. **Statistical analysis of simulations in $d = 1$ with symmetric interactions.** Simulations are performed at fixed $\rho_0 = \bar{\rho}$ for different values of the heterogeneity σ^2 , both in the absence (a-c) and in the presence (e-f) of an average motility inhibition. For each value of σ^2 the results of 15 simulations are shown as gray points, whose averages are shown using colored disks. White regions correspond to homogeneous simulations. Shaded regions correspond to fragmented or gregarious ecosystems and their colors encode the most probable fragmentation order parameter extracted from the simulations, using the same colorcode as in Fig. 2. Vertical dot-dashed blue lines are the theoretical predictions Eq. (8) (top) and Eq. (9) (bottom) for the transitions. The vertical black dashed line is the BBP transition $\sigma^2 = m^2$. The green dashed line is the prediction for the fragmentation order parameter, $F = 1$ in fragmented ecosystems and $F = \sigma^2/m^2$ below the BBP transition. Symbols measure the normalized standard deviations of the total-density histogram (blue, panels a&d) and of the single-strain density histograms (red, panels b&e). The data are normalized by the Poissonian fluctuations observed in homogeneous states. The green symbols show the most probable values of the fragmentation order parameter \bar{F} as defined in Fig. 1d-f. Parameters of the simulation: $N = 100$, $L_x = 30$, $\rho_0 = \bar{\rho} = 30$, $v_0 = 1$, $\tau_0 = 1$. In (a), $m = 0, \varphi = 20$, while in (b) $m = -1, \varphi = 45$. Further numerical details are reported in Methods.

The shaded regions in the panels of Fig. 3 correspond to phase separated simulations, defined as $\langle \Delta \rho_\mu \rangle > 2$. The transitions to community formation observed numerically coincide very well with the dot-dashed instability lines predicted by the theory.

To distinguish between gregarious and fragmented colonies, we also measured the fragmentation parameter F in inhomogeneous systems. We characterize a system by the most probable value \bar{F} extracted from the numerical measurement of the distribution $p(F)$ (See Fig. 1d-f).

In the absence of average inhibition ($m = 0$), we always observe fragmented ecosystems corresponding to $F = 1$ (Fig. 3c). In contrast, when $m < 0$, \bar{F} increases with σ^2 as the system transitions from a gregarious colony into a fragmented ecosystem (Fig. 3f). The cross-over to $F \simeq 1$ observed numerically corresponds well to the vertical dashed line, which indicates the BBP transition where our theory predicts that the most unstable mode corresponds to a fully fragmented ecosystem. Our microscopic simulations thus support the theoretical picture derived in Sec. III by applying random-matrix theory to the hydrodynamic description of the system.

IV. EXTENSION TO OTHER MOTILITY-REGULATION MECHANISMS

Let us now discuss how our results generalize beyond the model defined in Eqs. (1) and (2).

First, we note that our analysis directly extends to other motility-regulation functions beyond Eq. (1), such as $v_\mu(\{\rho_\mu\}) = v_0 \prod_\nu \phi_{\mu\nu}(\rho_\nu)$. Here, $\phi_{\mu\nu} \equiv \exp\{\kappa_{\mu\nu} \mathcal{S}[(\rho_\nu - \bar{\rho})/\varphi]\}$ represents a specific motility-regulation pathway that couples the strains μ and ν , leading to an overall factorized regulation of the motility. As shown in Supplementary Material and Methods, random motility regulation again leads to the emergence of a fragmented ecosystem and the change of regulating function mostly leads to different morphologies for the phase diagrams.

A second important ingredient of our model is how heterogeneity is taken into account in the motility regulation mechanism. Instead of the independent metabolic interactions considered above, which leads to i.i.d. $\kappa_{\mu\nu}$, one can also consider cases where motility is regulated by a single signaling field. We denote by γ_ν the production rate of the corresponding molecule by strain ν and by β_μ the susceptibility of strain μ , so that $\kappa_{\mu\nu} = \beta_\mu \gamma_\nu$ becomes a rank-one matrix. We refer to this case as the single-pathway motility-regulation network.

In Fig. 4b, we consider ecosystems where γ_ν and β_μ are distributed according to:

$$\gamma_\nu \sim \mathcal{N}(\bar{\gamma}/N, \sigma_\gamma^2/N), \quad \beta_\mu \sim \mathcal{N}(\bar{\beta}, \sigma_\beta^2), \quad (10)$$

where all coefficients $\bar{\gamma}, \bar{\beta}, \sigma_{\beta, \gamma}^2$ are taken to be $\mathcal{O}(1)$, so that the production rate is small while the strain susceptibility is $\mathcal{O}(1)$. When the system is gregarious at $\sigma_\beta^2 = \sigma_\gamma^2 = 0$, which corresponds to $\bar{\gamma}\bar{\beta} < -\varphi/\bar{\rho}$, our numerical simulations and theoretical computations detailed in SM show a transition into a fragmented phase upon increasing σ_β^2 , characterized by a fragmentation order parameter that can be approximated as

$$F \simeq \frac{\sigma_\beta^2}{\sigma_\beta^2 + \beta^2}. \quad (11)$$

Increasing the heterogeneity σ_β^2 of motility regulation

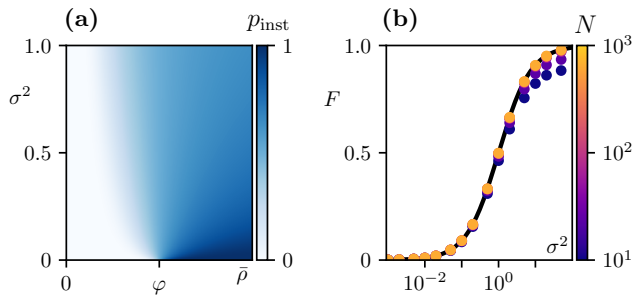


FIG. 4. **Single-pathway motility-regulation network.** (a) Heatmap of the probability p_{inst} for a homogeneous system to be unstable in the $(\bar{\rho}, \sigma^2)$ space. At large heterogeneity $\sigma^2 \equiv \sigma_\beta^2 = \sigma_\gamma^2$, p_{inst} always reaches the asymptotic value $1/2$. (b) Fragmentation parameter F obtained from numerical diagonalization of rank-one random matrices (points) versus the theoretical prediction of Eq. (11) (solid line). Data points are colored according to the number of strains N in the system. As predicted by Eq. (11), F increases with σ^2 : random interactions again promote community formation. Common parameters: $\bar{\beta} = -1, \bar{\gamma} = 1, \rho_0 = \bar{\rho}, \varphi = 10$. In (b), $\bar{\rho} = 30$.

thus again induces a fragmentation transition.

The topology of the motility-regulation network however induces an important difference with the metabolic case considered above. First, we predict a *finite* probability for a linear instability to occur for any $\sigma_{\gamma,\beta}^2 \neq 0$ (see Fig. 4a and SM). Then, the transition from gregarious to fragmented phase is replaced by a smooth crossover from $F = 0$ at $\sigma_\beta^2 = 0$ to $F = 1$ as $\sigma_\beta^2 \rightarrow \infty$, as shown in Fig. 4b. Note that this phenomenology extends to the case of $K \ll N$ signaling fields.

Then, throughout this article, we have considered the case in which the interactions and their heterogeneity scale as $\mathcal{O}(N^{-1})$. Biologically, this is motivated by the requirement to keep interactions finite in the limit of a large number of species. Mathematically, our results show that the case considered here is the most interesting scaling to study ecosystem fragmentation: the transition happens for $\sigma^2 \sim \mathcal{O}(1)$ and other scalings can be recovered by taking $\sigma^2 \rightarrow \infty$ and $\sigma^2 \rightarrow 0$, respectively (See SM for details).

Finally, we have studied a motility-regulation mechanism in which the speed of a strain depends on the local density of its peers through Eq. (1). Bacteria can also adapt their motilities to the local gradients of signaling fields, *e.g.* via chemotaxis. This is known to lead to a wealth of pattern-forming mechanisms [39, 60, 61] and it would thus be interesting to extend our results to such interactions. We expect our formalism to generalize straightforwardly to this case since the coarse-graining of such interactions lead to hydrodynamic equations very similar to Eq. (4) [53, 62].

V. DISCUSSION

In this work we have shown how random motility regulation promotes community formation in bacterial ecosystems. To this end, we have studied a model comprising $N \gg 1$ strains of run-and-tumble bacteria interacting via motility regulation. Using a combination of microscopic simulations and random matrix theory, we have shown that increasing the heterogeneity in the interaction network leads to the formation of segregated communities. This occurs both in the presence and in the absence of an average motility inhibition, and the phenomenology is robust with respect to the details of motility regulation. All in all, our work thus highlights the importance of motility regulation in the formation of communities within a microbial ecosystem, even when such a regulation is weak.

High-dimensional ecosystems are characterized by complex networks of interactions and we have argued that the emergence of fragmented ecosystems could arise either from direct motility regulation due to quorum sensing or from indirect regulation due to metabolic interactions. While we expect the latter to be most relevant in nature, the former offers an experimental platform to test our predictions in the future, using recent advances in engineered bacterial systems [41, 42].

Our results were established using a model that accounts for motility regulation using a density-based control of the bacteria swimming speed. We note that identical results could be obtained using models in which the tumble rates and durations depend on the local density, since they lead to hydrodynamic theory similar to Eq. (4) [53]. Furthermore, it is known that bacteria can also adapt their motility based on the gradients of some chemical fields, *e.g.* via chemotaxis. It would thus be interesting to extend our study to chemotactic interactions [39, 62] that are amenable to similar treatments.

In our model, we make the hypothesis of quenched interactions, assuming that the inter-strain couplings $\kappa_{\mu\nu}$ do not evolve in time. Nonetheless, if weak motility regulation stems as a side effect associated with metabolic pathways, it is plausible that the resulting interaction matrix fluctuates in time. It would thus be interesting to extend our work to the annealed case, accounting for the dynamics of the interaction matrix itself [63, 64]. Furthermore, we have considered equal strain compositions for the sake of simplicity. Random-matrix theory suggests that fluctuations in the species abundance could impact the phase equilibrium [49], which offers an interesting perspective for future work.

Finally, we have focused here on motility-induced community formation and shown how fragmentation may occur on relatively short time-scales due to active transport. On longer time scales, population dynamics will become relevant and other types of interactions, such as reproduction, cooperation, and competition for resources, will make the accessible phenomenology even

richer [31, 65, 66].

ACKNOWLEDGMENTS

The authors thank Victor Chardès and Peter Sollich for insightful discussions. AA acknowledges the support of ANR JCJC ‘‘SIDECAR’’ ANR-23-CE30-0012-01. JT and AD acknowledge the support of ANR THEMA and MIT MISTI GSF grant. AD was funded by an IDEX fellowship and by a postdoctoral contract at the Biochemistry department of the University of Geneva.

METHODS

Linearized field theory

To leading order in a gradient expansion, we approximate the speed of strain μ as $v_\mu(\mathbf{r}, \{\rho_\nu\}) \approx v_\mu(\{\rho_\nu(\mathbf{r})\})$. We then linearize the mean-field hydrodynamic theory for the density fields Eq. (4) around a well-mixed homogeneous profile ρ_0 to obtain N coupled diffusion equations for the strains: $\partial_t \rho_\mu = \mathcal{D}_{\mu\nu} \nabla_{\mathbf{r}}^2 \rho_\nu$, where the diffusivity matrix \mathcal{D} is given by Eq. (5). For the motility regulation defined by Eq. (1), $\mathcal{D}_{\mu\nu}$ becomes:

$$\mathcal{D}_{\mu\nu} = \mathcal{D}_\mu^0 \left[\delta_{\mu\nu} + \frac{\rho_0}{\varphi} \kappa_{\mu\nu} \mathcal{S}' \left(\sum_{\nu=1}^N \kappa_{\mu\nu} \frac{\rho_0 - \bar{\rho}}{\varphi} \right) \right],$$

with $\mathcal{S}'(x) = 1/\cosh^2(x)$. Further taking $\rho_0 = \bar{\rho}$ then gives Eq. Eq. (7).

Finally, for the alternative functional form $v_\mu = v_0 \prod_\nu \exp\{\kappa_{\mu\nu} \mathcal{S}[(\rho_\nu - \bar{\rho})/\varphi]\}$ considered in Sec. IV, Eq. (5) yields the following form for $\mathcal{D}_{\mu\nu}$:

$$\mathcal{D}_{\mu\nu} = \mathcal{D}_\mu^0 \left[\delta_{\mu\nu} + \frac{\rho_0}{\varphi} \kappa_{\mu\nu} \mathcal{S}' \left(\frac{\rho_0 - \bar{\rho}}{\varphi} \right) \right],$$

so that Eq. (7) follows again from $\rho_0 = \bar{\rho}$.

Microscopic simulations

Here we describe the algorithm used to perform particle-based simulations in $1d$ and $2d$ continuous space. In the following, the notation (i, μ) denotes particle i of strain μ , $\mathbf{r}_{i,\mu}$ its position and $\mathbf{u}_{i,\mu}$ its orientation.

We initialize the system in a homogeneous configuration at time $t = 0$, and, for each particle, we draw the next tumbling time $t_{i,\mu}$ from the exponential distribution $p_t(t_i) \equiv \exp(-t_i/\tau_0)/\tau_0$, where τ_0 is the persistence time. Particle positions and orientations between times t and $t + dt$ are then updated as follows. At each time step, we first measure the coarse-grained density fields $\{\tilde{\rho}_{i,\nu}\}$ as $\tilde{\rho}_{i,\nu} \equiv \sum_{(j,\nu)} K(|\mathbf{r}_{i,\mu} - \mathbf{r}_{j,\nu}|)$, where $K(r)$ is a normalized symmetric kernel given by $K(r) =$

$Z^{-1} \exp[-\frac{r^2}{\tau_0^2 - r^2}] \Theta(r - r_0)$. We then determine the instantaneous self-propulsion speeds as $v_{i,\mu} = v(\{\tilde{\rho}_{i,\nu}\})$.

Next, for each particle we check whether the next tumbling event $t_{i,\mu}$ occurs in $[t, t + dt)$. If so, we first evolve the particle position $\mathbf{r}_{i,\mu}$ in the interval $dt' = t_{i,\mu} - t$ as $\mathbf{r}_{i,\mu}(t + dt') = \mathbf{r}_{i,\mu}(t) + v(\{\tilde{\rho}_{i,\nu}\}) \mathbf{u}_{i,\mu} dt'$. We then draw a new orientation $\mathbf{u}'_{i,\mu}$ uniformly at random, and update the next tumbling time as $t_{i,\mu} \rightarrow t_{i,\mu} + \Delta t_{i,\mu}$, where $\Delta t_{i,\mu}$ is drawn from the exponential distribution p_t . We then iterate this process until the particle’s position has been evolved up to time $t + dt$.

Analysis of $1d$ simulations

To test our theoretical predictions shown in Fig. 2, we use simulations of one-dimensional systems, both in the presence of average motility inhibition ($m = -1$) and in its absence ($m = 0$). We simulate $N = 100$ species on a domain of length $L_x = 30$, setting the bare self-propulsion speed to $v_0 = 1$, the persistence time $\tau_0 = 1$, and the interaction radius $r_0 = 1$. We fix the density per species at $\rho_0 = \bar{\rho} = 30$ and choose $\varphi = 20$ for $m = 0$, $\varphi = 45$ for $m = -1$. For each value of σ^2 , we perform $K = 15$ simulations. To analyze the resulting data, we divide the space in boxes of width $dx = 1$ and, for each box i , we build a vector of local strain densities $\boldsymbol{\rho}^{(i)} = (\rho_1^{(i)}, \dots, \rho_N^{(i)})$. We then define the (rescaled) total density $\rho_t^{(i)} = N^{-1} \sum_\mu \rho_\mu^{(i)}$ inside box i and the local fragmentation parameter $F^{(i)} = 1 - N^{-1} \left(\sum_\mu \rho_\mu^{(i)} \right)^2 / |\boldsymbol{\rho}^{(i)}|^2$. By averaging over several time samples, we then build the histogram for each species’ density $p(\rho_\mu)$, the total-density histogram $p(\rho_t)$, and the fragmentation-parameter histogram $p(F)$.

To distinguish between different phases we then compute the following quantities:

$$\Delta \rho_t \equiv \sqrt{\frac{\text{Var}[\rho_t]}{\rho_0/(N dx)}}, \quad (12)$$

$$\langle \Delta \rho_\mu \rangle \equiv \frac{1}{N} \sum_{\mu=1}^N \sqrt{\frac{\text{Var}[\rho_\mu]}{\rho_0/dx}}, \quad (13)$$

$$\bar{F} \equiv \arg \max[p(F)], \quad (14)$$

where the variances $\text{Var}[\cdot]$ are computed using the corresponding histogram. In the absence of phase separation, in both single-species and total-density histograms the variance is dictated by Poissonian fluctuations, so that both $\Delta \rho_t$ and $\langle \Delta \rho_\mu \rangle$ should be close to 1. Therefore, deviations of these quantities from 1 indicate, respectively, the occurrence of phase-separation for the total density and for each species separately. We use $\Delta \rho_t > 2$ as a criterion to distinguish between homogeneous and

phase-separated profiles.

For the simulations reported Fig. 3, we obtain the green disks by averaging \bar{F} over phase-separated simulations. Using these values we build the heatmap for \bar{F} in

Fig. 3c,e using the same colorcode as in Fig. 2. Between two data points, colors are obtained by linear interpolation of our numerical data.

-
- [1] M. Kopp, Speciation and the neutral theory of biodiversity: Modes of speciation affect patterns of biodiversity in neutral communities., *Bioessays* **32**, 564 (2010).
- [2] S. P. Hubbell, *The unified neutral theory of biodiversity and biogeography (MPB-32)* (Princeton University Press, 2011).
- [3] S. Allesina, Going big, *Unsolved problems in ecology*, 374 (2020).
- [4] M. A. Leibold, M. Holyoak, N. Mouquet, P. Amarasekare, J. M. Chase, M. F. Hoopes, R. D. Holt, J. B. Shurin, R. Law, D. Tilman, *et al.*, The metacommunity concept: a framework for multi-scale community ecology, *Ecology letters* **7**, 601 (2004).
- [5] D. S. Wilcove and M. Wikelski, Going, going, gone: is animal migration disappearing, *PLoS biology* **6**, e188 (2008).
- [6] K. J. Gaston, Global patterns in biodiversity, *Nature* **405**, 220 (2000).
- [7] C.-H. Tsai, T. Miki, C.-W. Chang, K. Ishikawa, S. Ichise, M. Kumagai, and C.-h. Hsieh, Phytoplankton functional group dynamics explain species abundance distribution in a directionally changing environment, *Ecology* **95**, 3335 (2014).
- [8] L. Dethlefsen, S. Huse, M. L. Sogin, and D. A. Relman, The pervasive effects of an antibiotic on the human gut microbiota, as revealed by deep 16s rRNA sequencing, *PLoS biology* **6**, e280 (2008).
- [9] C. Ratzke and J. Gore, Modifying and reacting to the environmental pH can drive bacterial interactions, *PLoS biology* **16**, e2004248 (2018).
- [10] M. Daniels, S. van Vliet, and M. Ackermann, Changes in interactions over ecological time scales influence single-cell growth dynamics in a metabolically coupled marine microbial community, *The ISME Journal* **17**, 406 (2023).
- [11] G. Hardin, The competitive exclusion principle: an idea that took a century to be born has implications in ecology, economics, and genetics., *science* **131**, 1292 (1960).
- [12] J. P. Grime, Competitive exclusion in herbaceous vegetation, *Nature* **242**, 344 (1973).
- [13] P.-Y. Ho, T. H. Nguyen, J. M. Sanchez, B. C. DeFelice, and K. C. Huang, Resource competition predicts assembly of gut bacterial communities in vitro, *Nature Microbiology*, 1 (2024).
- [14] G. Barabás, M. J. Michalska-Smith, and S. Allesina, The effect of intra-and interspecific competition on coexistence in multispecies communities, *The American Naturalist* **188**, E1 (2016).
- [15] J. Friedman, L. M. Higgins, and J. Gore, Community structure follows simple assembly rules in microbial microcosms, *Nature ecology & evolution* **1**, 0109 (2017).
- [16] B. H. Good, M. J. McDonald, J. E. Barrick, R. E. Lenski, and M. M. Desai, The dynamics of molecular evolution over 60,000 generations, *Nature* **551**, 45 (2017).
- [17] M. T. Pearce, A. Agarwala, and D. S. Fisher, Stabilization of extensive fine-scale diversity by ecologically driven spatiotemporal chaos, *Proceedings of the National Academy of Sciences* **117**, 14572 (2020).
- [18] J. Hu, D. R. Amor, M. Barbier, G. Bunin, and J. Gore, Emergent phases of ecological diversity and dynamics mapped in microcosms, *Science* **378**, 85 (2022).
- [19] I. A. Hattton, O. Mazzarisi, A. Altieri, and M. Smerlak, Diversity begets stability: Sublinear growth and competitive coexistence across ecosystems, *Science* **383**, eadg8488 (2024).
- [20] J. Vano, J. Wildenberg, M. Anderson, J. Noel, and J. Sprott, Chaos in low-dimensional lotka-volterra models of competition, *Nonlinearity* **19**, 2391 (2006).
- [21] S. Vet, S. de Buyl, K. Faust, J. Danckaert, D. Gonze, and L. Gelens, Bistability in a system of two species interacting through mutualism as well as competition: Chemostat vs. lotka-volterra equations, *PloS one* **13**, e0197462 (2018).
- [22] A. E. Blanchard and T. Lu, Bacterial social interactions drive the emergence of differential spatial colony structures, *BMC systems biology* **9**, 1 (2015).
- [23] J. H. van Opheusden, L. Hemerik, M. van Opheusden, and W. van der Werf, Competition for resources: complicated dynamics in the simple tilman model, *SpringerPlus* **4**, 1 (2015).
- [24] O. Hallatschek, P. Hersen, S. Ramanathan, and D. R. Nelson, Genetic drift at expanding frontiers promotes gene segregation, *Proceedings of the National Academy of Sciences* **104**, 19926 (2007).
- [25] K. S. Korolev, M. Avlund, O. Hallatschek, and D. R. Nelson, Genetic demixing and evolution in linear stepping stone models, *Reviews of modern physics* **82**, 1691 (2010).
- [26] J. Hofbauer and K. Sigmund, *Evolutionary games and population dynamics* (Cambridge university press, 1998).
- [27] A. J. Lotka, *Analytical theory of biological populations* (Springer Science & Business Media, 2013).
- [28] B. Bloxham, H. Lee, and J. Gore, Diauxic lags explain unexpected coexistence in multi-resource environments, *Molecular Systems Biology* **18**, e10630 (2022).
- [29] B. Bloxham, H. Lee, and J. Gore, Biodiversity is enhanced by sequential resource utilization and environmental fluctuations via emergent temporal niches, *PLOS Computational Biology* **20**, e1012049 (2024).
- [30] M. Tikhonov and R. Monasson, Collective phase in resource competition in a highly diverse ecosystem, *Physical review letters* **118**, 048103 (2017).
- [31] G. Bunin, Ecological communities with lotka-volterra dynamics, *Physical Review E* **95**, 042414 (2017).
- [32] G. Biroli, G. Bunin, and C. Cammarota, Marginally stable equilibria in critical ecosystems, *New Journal of Physics* **20**, 083051 (2018).
- [33] A. Altieri, F. Roy, C. Cammarota, and G. Biroli, Properties of equilibria and glassy phases of the random lotka-volterra model with demographic noise, *Physical Review Letters* **126**, 258301 (2021).

- [34] A. Altieri and G. Biroli, Effects of intraspecific cooperative interactions in large ecosystems, *SciPost Physics* **12**, 013 (2022).
- [35] W. Cui, R. Marsland III, and P. Mehta, Effect of resource dynamics on species packing in diverse ecosystems, *Physical review letters* **125**, 048101 (2020).
- [36] E. Blumenthal, J. W. Rocks, and P. Mehta, Phase transition to chaos in complex ecosystems with nonreciprocal species-resource interactions, *Physical Review Letters* **132**, 127401 (2024).
- [37] A. Salvatore, F. Aguirre-López, and R. Zakine, Patterns robust to disorder in spatially-interacting generalized lotka-volterra ecosystems, arXiv preprint arXiv:2501.03809 (2025).
- [38] P. W. Anderson, More is different: Broken symmetry and the nature of the hierarchical structure of science., *Science* **177**, 393 (1972).
- [39] E. O. Budrene and H. C. Berg, Complex patterns formed by motile cells of *escherichia coli*, *Nature* **349**, 630 (1991).
- [40] M. B. Miller and B. L. Bassler, Quorum sensing in bacteria, *Annual Reviews in Microbiology* **55**, 165 (2001).
- [41] C. Liu, X. Fu, L. Liu, X. Ren, C. K. Chau, S. Li, L. Xiang, H. Zeng, G. Chen, L.-H. Tang, *et al.*, Sequential establishment of stripe patterns in an expanding cell population, *Science* **334**, 238 (2011).
- [42] A. Curatolo, N. Zhou, Y. Zhao, C. Liu, A. Daerr, J. Tailleur, and J. Huang, Cooperative pattern formation in multi-component bacterial systems through reciprocal motility regulation, *Nature Physics* **16**, 1152 (2020).
- [43] B. E. Morris, R. Henneberger, H. Huber, and C. Moissl-Eichinger, Microbial syntrophy: interaction for the common good, *FEMS microbiology reviews* **37**, 384 (2013).
- [44] G. D'Souza, S. Shitut, D. Preussger, G. Yousif, S. Waschina, and C. Kost, Ecology and evolution of metabolic cross-feeding interactions in bacteria, *Natural product reports* **35**, 455 (2018).
- [45] A. Alvarado, W. Behrens, and C. Josenhans, Protein activity sensing in bacteria in regulating metabolism and motility, *Frontiers in microbiology* **10**, 3055 (2020).
- [46] H. C. Berg, *E. coli in Motion* (Springer, 2004).
- [47] R. P. Sear and J. A. Cuesta, Instabilities in complex mixtures with a large number of components, *Physical review letters* **91**, 245701 (2003).
- [48] K. Shrinivas and M. P. Brenner, Phase separation in fluids with many interacting components, *Proceedings of the National Academy of Sciences* **118**, e2108551118 (2021).
- [49] F. C. Thewes, M. Krüger, and P. Sollich, Composition dependent instabilities in mixtures with many components, *Physical Review Letters* **131**, 058401 (2023).
- [50] L. Parkavousi, N. R. Golestanian, S. Saha, *et al.*, Enhanced stability and chaotic condensates in multi-species non-reciprocal mixtures, arXiv preprint arXiv:2408.06242 (2024).
- [51] G. Garcia Lorenzana and A. Altieri, Well-mixed lotka-volterra model with random strongly competitive interactions, *Physical Review E* **105**, 024307 (2022).
- [52] M. E. Cates and J. Tailleur, Motility-induced phase separation, *Annu. Rev. Condens. Matter Phys.* **6**, 219 (2015).
- [53] A. Dinelli, J. O'Byrne, and J. Tailleur, Fluctuating hydrodynamics of active particles interacting via chemotaxis and quorum sensing: static and dynamics, arXiv preprint arXiv:2402.05072 (2024).
- [54] S. F. Edwards and R. C. Jones, The eigenvalue spectrum of a large symmetric random matrix, *Journal of Physics A: Mathematical and General* **9**, 1595 (1976).
- [55] J. Baik, G. Ben Arous, and S. Péché, Phase transition of the largest eigenvalue for nonnull complex sample covariance matrices, *The Annals of Probability* (2005).
- [56] D. Paul, Asymptotics of sample eigenstructure for a large dimensional spiked covariance model, *Statistica Sinica* , 1617 (2007).
- [57] F. Benaych-Georges and R. R. Nadakuditi, The eigenvalues and eigenvectors of finite, low rank perturbations of large random matrices, *Advances in Mathematics* **227**, 494 (2011).
- [58] G. Livan, M. Novaes, and P. Vivo, Introduction to random matrices theory and practice, *Monograph Award* **63**, 54 (2018).
- [59] E. P. Wigner, On the distribution of the roots of certain symmetric matrices, *Annals of Mathematics* **67**, 325 (1958).
- [60] E. Ben-Jacob, I. Cohen, O. Shochet, I. Aranson, H. Levine, and L. Tsimring, Complex bacterial patterns, *Nature* **373**, 566 (1995).
- [61] M. P. Brenner, L. S. Levitov, and E. O. Budrene, Physical mechanisms for chemotactic pattern formation by bacteria, *Biophysical journal* **74**, 1677 (1998).
- [62] J. O'Byrne and J. Tailleur, Lamellar to micellar phases and beyond: When tactic active systems admit free energy functionals, *Physical Review Letters* **125**, 208003 (2020).
- [63] S. Suweis, F. Ferraro, C. Grilletta, S. Azaele, and A. Maritan, Generalized lotka-volterra systems with time correlated stochastic interactions, *Physical Review Letters* **133**, 167101 (2024).
- [64] A. Altieri and S. De Monte, Unveiling complexity: Statistical physics approaches to ecological communities, *EPL Perspectives*, to appear (2025).
- [65] R. M. May, Simple mathematical models with very complicated dynamics, *Nature* **261**, 459 (1976).
- [66] M. O. Lavrentovich and D. R. Nelson, Asymmetric mutualism in two-and three-dimensional range expansions, *Physical review letters* **112**, 138102 (2014).